NUMERICAL SIMULATIONS OF A NOVEL ELECTRICAL HEATED BRICK FIRING KILN

Manuel Schieder[1]*, Julian Unterluggauer[1], Stefan Puskas[2], Stefan Vogt[2]

[1]AIT Austrian Institute of Technology GmbH, Center for Energy, Vienna, Vienna, Austria

[2]Wienerberger AG, Vienna, Vienna, Austria

*Corresponding Author: manuel.schieder@ait.ac.at

ABSTRACT

To achieve the goal of a sustainable and CO_2-neutral future, it is crucial for industries with high carbon footprints, such as the brick manufacturing industry, to utilize sustainable alternatives to natural gas. One of the available options is the use of carbon-free electricity. In Austria world leading brick manufacturer Wienerberger AG is currently building a kiln, which produces all its heat by electricity. The use of electricity fundamentally alters the firing process and therefore a novel approach to the kiln design is applied. The electrically heated kiln uses several heating elements on top, on the sides, and on the floor in each kiln zone to heat the bricks. Additionally, TOREtech nozzles are used to increase turbulence and enhance heat transfer. Computational fluid dynamics (CFD), using the commercial software Ansys Fluent, is used to analyze the heat distribution in the kiln zone, as well as to shed light on the fatigue life of the heating elements.
The results show that even in the most critical zone of the kiln, the applied heating elements are sufficient to heat the brick in the specified time, while also staying within their operating limits. The heat distribution of the kiln and the bricks is comparable and even better than in a state-of-the-art gas-fired kiln.

1 INTRODUCTION

As the need for CO_2 reduction is one of the most pressing concerns for humanity, CO_2 emitting industries must react immediately and without delay. The construction- and buildings industry is one of the greatest raw material users and this demand is still rising due to increasing living standards and the need for more infrastructure (Valdes et al., 2020). Already more than 5000 years ago bricks were used as a construction material, starting their journey towards one of the most popular construction materials (Krishna, 2021). However, state-of-the-art brick production relies on high amounts of natural gas for the drying- and firing process. Therefore, to decarbonize these processes, natural gas must be substituted with a sustainable alternative. Brick manufacturers are making significant efforts to reduce CO_2 emission in order to achieve their goal of CO_2 neutrality. Due to the questionable availability of sustainable fuel alternatives like hydrogen, a different approach needs to be applied (Mödinger, 2021). A switch to electricity-powered kilns provides a promising option, as renewables like on-site photovoltaic in combination with hydropower, wind energy, and other renewable sources from the grid can cover the power demand.
However, the switch from gas-fired kilns to electrically heated kilns fundamentally alters the firing process and therefore presents various challenges. One of the key questions is how to reach a sufficient heat transfer from the heating elements to the bricks. Radiation alone is not as effective as enforced convection, which comes with more uniform heating and as a result a better product quality. Therefore, to mimic the effect of gas burners, which introduce turbulence and thereby achieve a more uniform heat distribution, TOREtech nozzles are used (Puskas, 2020). The TOREtech nozzle operates on a jet pump concept, using a high-velocity jet to draw in kiln air. The air mixture is then directed into the firing zone to enhance mixing. (Pichler, 2021).

https://doi.org/10.52202/077185-0135

Additionally, the gap between the bricks and the kiln wall is kept minimal, to force most of the airflow through the brick holes.
For the investigation of the heat transfer and the flow field inside the tunnel kiln CFD is used, as it is a proven tool for such problems. Refaey and Specht (2013) used CFD to study the impact of radial nozzles, which generate better mixing in tunnel kilns. In a different study, Refaey et al. (2021) investigated the effect of different lattice brick settings on the convective heat transfer, using CFD. Moreover, Abou-Ziyan et al. (2018) found that when a uniform flow field is reached in a tunnel kiln, depending on the brick lattice settings, the convective heat transfer can be enhanced by up to 27%.
In this work, the heat transfer (convection and radiation) of electric heating elements in a tunnel kiln is investigated using CFD. These main issues are addressed:

- The temperature spread in the brick stack.
- The resulting temperatures of the heating elements, to obtain an estimate for their fatigue life.

2 NUMERICAL MODEL

In the investigated tunnel kiln the bricks need to reach at least 960°C to complete the brick firing process. Once they have reached this temperature, they are cooled down in a controlled manner. The bricks are transported through the tunnel kiln batch-wise as stacks, consisting of several rows of bricks. To guarantee the highest product quality the bricks are heated up slowly to reach a uniform temperature distribution. Therefore, the tunnel kiln is divided into several zones in which each brick stack stops for 10-15 minutes to heat up or cool down uniformly. The zones are divided into m heating zones, in which the bricks slowly heat up, and n cooling zones in which the bricks cool down in a controlled manner until they reach temperatures close to the ambient temperature. This results in a total kiln length of 80m and a width of 6m. The heat gets introduced to each heating zone with heating elements, located on the sides, the top, and underneath the bricks. Additionally, air gets blown in at the end of the tunnel kiln, which cools the bricks in the cooling zones, and heats the bricks in the heating zones. To introduce turbulence and increase the heat transfer, two TOREtech nozzles are placed in each zone. Figure 1 shows a schematic drawing of the tunnel kiln.

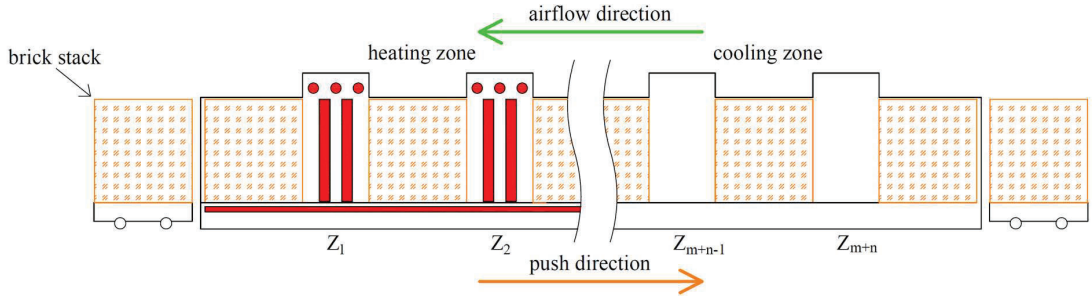

Figure 1: Schematic drawing of the tunnel kiln, showing the brick stacks in orange and the heating elements in red.

2.1 Computational Domain

To model heat transfer and analyze the behavior of the electrical heating elements, the most critical zone is simulated. The domain comprises a single row of bricks at the beginning and the end of the considered zone, as well as the entire firing zone between the stacks which contains the heating elements and the TOREtech nozzle. As can be seen in Figure 2, the domain is sliced to take advantage of symmetry. This leads to a reduction in computation time.
The firing zone consists of three heating elements at the top, two on the side, and 40 smaller heating elements at the bottom. The active area of the heating elements is marked in red in Figure 2(c). The TOREtech nozzle, which is located between the top heating elements, sucks in air at the top of the firing zone creating additional convection around the top elements, while the air inlet of the nozzle is positioned beneath the heating elements. For details see Figure 2. Solid panels are in place to protect

https://doi.org/10.52202/077185-0135

the side elements and prevent the bricks from getting hooked into the side chamber. Moreover, panels are positioned to prevent any material from reaching the bottom heating elements.

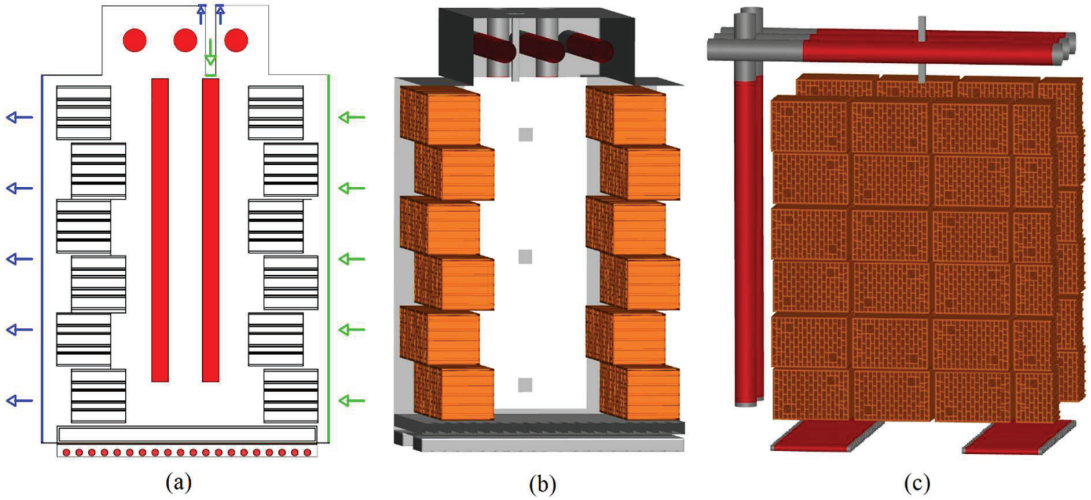

Figure 2: Computational domain. (a): Schematic drawing of the computational domain with zone- and nozzle inlet in green, zone- and nozzle outlet in blue, and heating elements in red. (b) CFD domain. (c) CFD domain with hidden walls, showing the active part of the heating elements in red.

2.2 CFD-Setup

The CFD simulations are performed using the commercial software Ansys® Fluent, Release 23.2 (ANSYS, Inc., 2023). To model the turbulent airflow Reynolds averaged (RANS) and further unsteady Reynolds averaged Navier–Stokes equations (URANS), using the shear stress transport (SST) model are used. Radiation is modeled by the surface-to-surface (S2S) model with a maximum number of 5 radiation iterations. The advection term is discretized by a second-order upwind scheme, while turbulence is approximated by a first-order scheme. In the steady state case around 1000 iterations are performed with an automatic time-stepping approach to reach convergence faster. Convergence is checked by the residuals and additionally, key variables are monitored over the iterations. For the transient simulations, a time step size of 0.02s with a maximum of eight iterations per timestep is used. This timestep size was determined by preliminary tests and has been proven sufficient with regard to residuals and the convergence of key variables, such as temperatures. This results in an average CFL number of 7.79.

The air inside the kiln is treated as an ideal gas with temperature-dependent material properties. For the brick, a constant density of 1650 kg/m³ with a thermal conductivity of 0.26 W/(mK) is used. The specific heat capacity is assumed to be linear between 0 and 1000°C with values of 900 to 1000 J/(kgK). The temperature of the brick is held constant at 931°C in the steady state simulation and for the transient simulation, this temperature is used as the initial temperature. The emissivity factors vary depending on the used material, ranging from 0.75-0.85. Boundary conditions are listed in Table 1.

Table 1: Boundary conditions.

position	type	value
zone inlet	velocity	mapped profile, 1.07 kg/s, 960°C
nozzle inlet	mass flow	0.019 kg/s, 900°C
zone outlet	gauge pressure	0 Pa
nozzle outlet	mass flow	0.017 kg/s
top elements	power	18.5 kW

https://doi.org/10.52202/077185-0135

side elements	power	17.3 kW
bottom elements	power	11.8 kW

To keep simulation times and the computational demand reasonable, simplifications must be made. Besides using symmetry, only one row of bricks is modeled, and some geometry simplifications are made. As mentioned in Table 1, the velocity profile in the zone inlet is a mapped profile. This profile is generated following these steps:

1. Simulation of the whole domain supplying the given mass flow on the zone inlet (block profile).
2. After the simulation is converged, read the velocity profile behind the first row of bricks.
3. Check the difference in mass flow rate of the resulting velocity profile and scale it accordingly.*
4. Use the scaled velocity profile as a velocity inlet condition for the next simulation.
5. Repeat steps 2 – 4 to get an approximation of the velocity field after the given number of brick rows.

*The difference in mass flow rate occurs because the air cools down as it passes the bricks, resulting in an increased density and therefore decreased velocity. To account for the density difference, the velocity field needs to be scaled.

2.3 Geometry and Grid

In the design process of the grid, some challenges could be identified. Since the domain is relatively big compared to some details that need to be modeled, e.g., the flow through the brick holes, the number of cells needs to be high to guarantee grid independence. The used grid for all the simulations has a cell count of around 22.5 million. To keep the computation time in a reasonable range, especially for the transient simulation, the usage of grid interfaces is avoided. Moreover, the mesh consists of mostly hexahedral elements (97%) with just a low number of quad-based pyramids (3%) as a filler. To generate such a grid, the domain needs to be sliced into several thousand bodies with different shapes and sizes. Figure 3 shows a detailed view of the grid in a single brick. As can be seen, every part of the brick has at least two cells in each direction. This is necessary to model the heat transfer within the bricks properly. In the brick holes, the cells get smaller close to the walls, and therefore the flow field can be resolved with sufficient accuracy. In total each brick consists of around 165,000 cells, including the fluid domain inside the holes. As can be seen in Figure 2(b), the brick is only a small part of the whole simulation domain and therefore, to save computation time, the brick cannot be modeled in greater detail. However, this resolution proved to be sufficient.
In Table 2, some quality metrics of the used grid are displayed. The average y^+ value is around 2 with a maximum of 15. These are suitable values for the SST model with enhanced wall functions as proposed by Menter (1994).

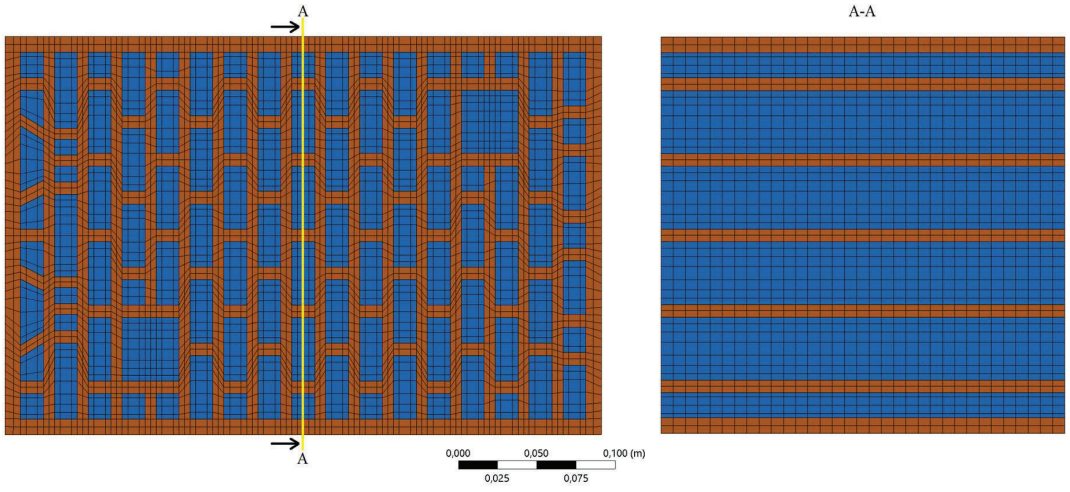

Figure 3: Detail view of the grid in the bricks. The domain of the bricks is depicted in brown and the domain of the air in blue.

https://doi.org/10.52202/077185-0135

Table 2: Quality metrics of the used grid.

metric	Value
max. skewness	0.87
min. jacobian ratio (Gauss points)	0.397
max. aspect ratio	13.7
min. element quality	0.142
average y^+	2
max y^+	15

3 GRID INDEPENDENCE STUDY

To verify that the solution is independent of the grid, a grid convergence study is conducted. Since there is no standard procedure to guarantee grid independence, it can be chosen by a variety of methods (Lee et al., 2020). A widely used and evaluated way to determine grid independence is the Grid Convergence Method (GCI) which is based on the Richardson extrapolation (RE) and was proposed by Celik. et al. (2008).
Due to the size and complexity of the grid, simplifications for the grid independence study are taken. The grid is refined two times, whereas only the chambers in which the heating elements are located are refined. This was done because previous tests have shown that these are the most critical areas and therefore the complex process of refinement over the whole domain could be avoided.

3.1 Results

Since the main objective of the study is the analysis of the heating element temperatures, the maximum temperature of the bottom elements $T_{max,bot}$ as well as the maximum temperature of the top elements $T_{max,top}$ are used as key variables for the grid independence study. In Table 3 the most important results are displayed.

Table 3: Selected results of the grid independence study.

	$T_{max,bot}$	$T_{max,top}$
N_1; N_2; N_3	$2.18*10^8$, $4.42*10^7$; $2.25*10^7$	
r_{21}	1.70	
r_{32}	1.25	
e_a^{21}	$2.8*10^{-2}$ %	$4.4*10^{-3}$ %
e_a^{32}	$1.6*10^{-1}$ %	$1.9*10^{-2}$ %
GCI^{21}_{fine}	$4.1*10^{-4}$ %	$1.2*10^{-4}$ %
GCI^{32}_{coarse}	$3.5*10^{-2}$ %	$5.7*10^{-3}$ %

In Figure 4 the numerical solution for each key variable φ is compared with the extrapolated numerical solution of this variable φ_{ext}. The coarse grid, with the highest representative cell size, is very close to the extrapolated solution with a deviation below 0.2%. It can also be seen, that refining the mesh has a greater impact on the accuracy of the maximum temperature of the bottom elements, than on that of the top elements. However, the gain in accuracy by using a finer grid, compared to the numerical cost is too low. Furthermore, a finer grid would lead to the need for a finer time step for the transient simulations to keep the CFL number low. This would increase the computation time additionally.

https://doi.org/10.52202/077185-0135

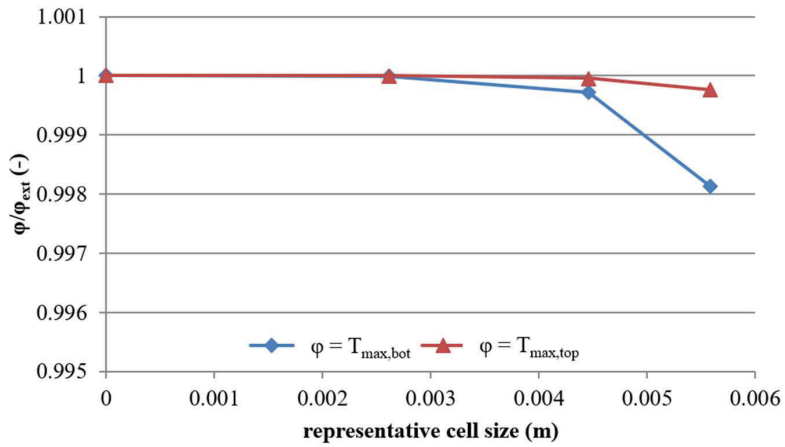

Figure 4: Ratio of the key variables φ with their extrapolated result φ_{ext} from all three grids, plotted against the representative cell size h.

4 RESULTS

In this section, the results of all simulations are presented and discussed. At first, the results of the steady-state simulation will be presented, followed by the results of the transient simulation. The heating element temperatures are always displayed in relation to their highest permissible operating temperature, using the following equations.

$$\gamma_{max} = \frac{T_{HE,max}\ [K]}{T_{HE,limit}\ [K]}$$

$$\gamma_{av} = \frac{T_{HE,av}\ [K]}{T_{HE,limit}\ [K]}$$

Here $T_{HE,max}$ and $T_{HE,av}$ denote the maximum and average temperature of a heating element. $T_{HE,limit}$ denotes the highest permissible operating temperature for the heating elements. This temperature limit was determined by the manufacturer through heating tests, ensuring durability by maintaining temperatures below this limit.

4.1 Steady state simulations

To determine the maximum temperature of the heating elements which is necessary to transport the given amount of heat into the bricks, a steady state simulation is carried out. To get a better understanding of the flow field inside the kiln zone and to determine the influence of the TOREtech nozzle, a contour plot at the location of the nozzle is shown in Figure 5.

As mentioned in the previous section, the inlet velocity profile for the kiln zone is a mapped profile and the effect of that can be seen in Figure 5(b). The results also show that the TOREtech nozzle ensures mixing over the whole height of the kiln, while also creating additional convection around the top elements.

In Figure 6 a couture plot of γ, the ratio of the static temperature relative to the permissible temperature of the heating elements, is displayed. The averaged and maximum values for the heating elements are summarized in Table 4. The effect of the introduced convection from the nozzle around the top elements can be seen, as those are cooler compared to the side elements. It can be concluded that for the current setup, the heating elements can supply the given amount of heat to the bricks while staying below their highest permissible operating temperature.

https://doi.org/10.52202/077185-0135

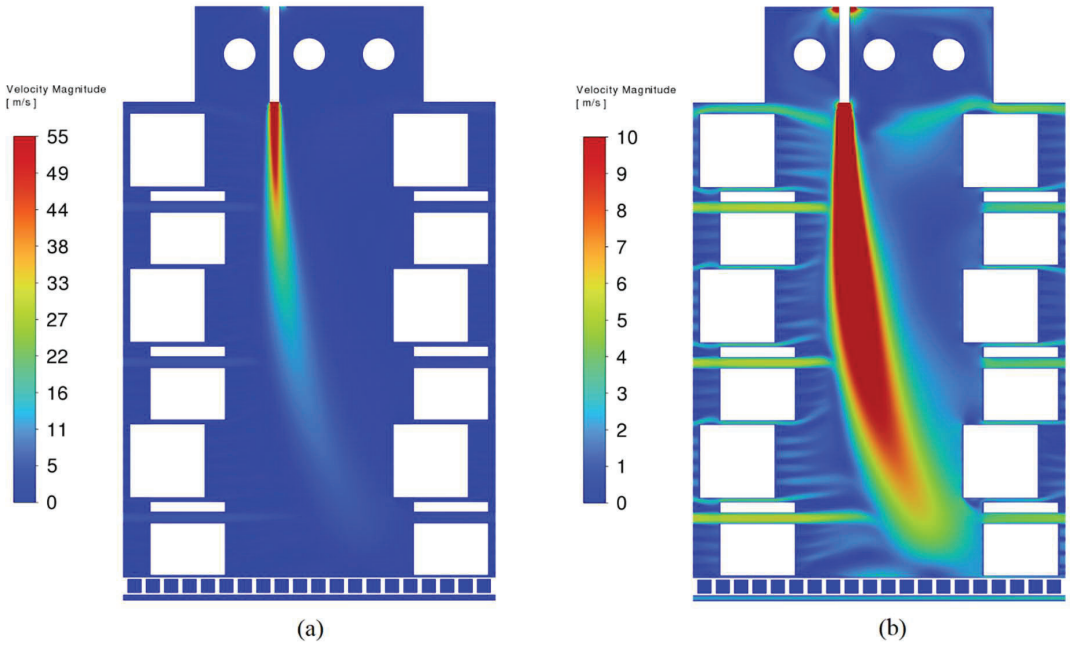

Figure 5: Contour plot of the velocity magnitude (m/s) located at the TOREtech nozzle, using different scalings.

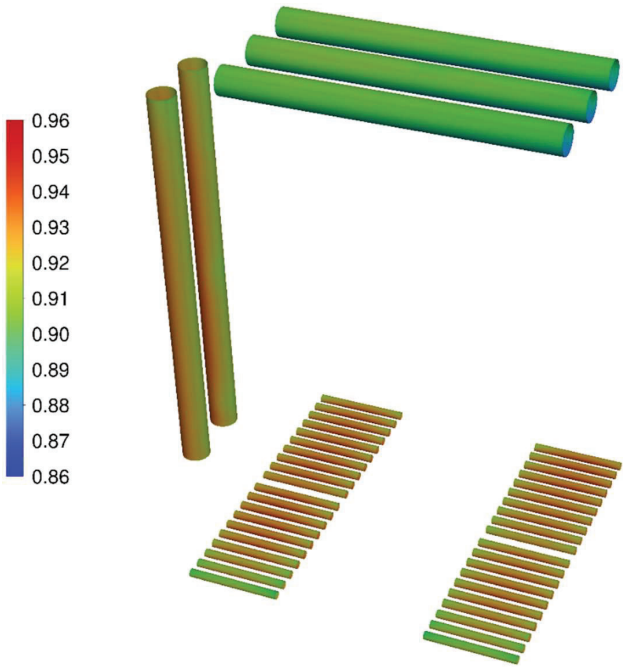

Figure 6: Contour plot of the static temperature relative to the permissible temperature of the heating elements γ (-).

https://doi.org/10.52202/077185-0135

Table 4: Maximum and average values of the static temperature relative to the permissible temperature of the heating elements γ (-).

	top	side	bottom
γ_{max}	0.91	0.94	0.96
γ_{av}	0.90	0.93	0.93

4.2 Transient simulations

To determine transient heating behavior, 10 minutes of heating time are simulated. In Figure 7 the minimum, average, and maximum temperature of the brick is depicted. The boundary zones of the stack are heating up much faster due to enforced convection and a stronger impact of radiation. Additionally, bricks are designed to insulate and therefore they have a low thermal conductivity, leading to a slow heat transfer inside the brick. However, after ten minutes the average temperature of the brick is already above 960°C and the temperature spread, $T_{brick,max} - T_{brick,min}$, in the brick stack is around 80K, which is comparable to natural gas-fired kilns and sufficient for product requirements.

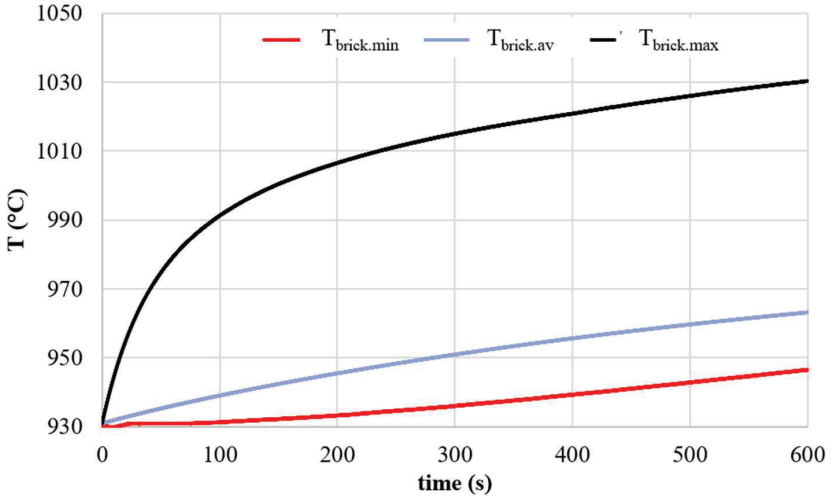

Figure 7: Brick temperature in the simulated kiln zone.

Figure 8 shows the resulting temperature of the heating elements relative to their highest permissible operating temperature. Values below the operating limit should allow continuous operation without the risk of early lifetime failure. During the whole process, the temperatures remain on a high level but do not exceed the limits. Based on the heating element temperatures, even higher electrical heating values would be possible without risking fatigue. However, the desired average temperature inside the brick is already reached and more power input would not only lead to faster firing times but also to a wider temperature spread which is critical in terms of product quality.

https://doi.org/10.52202/077185-0135

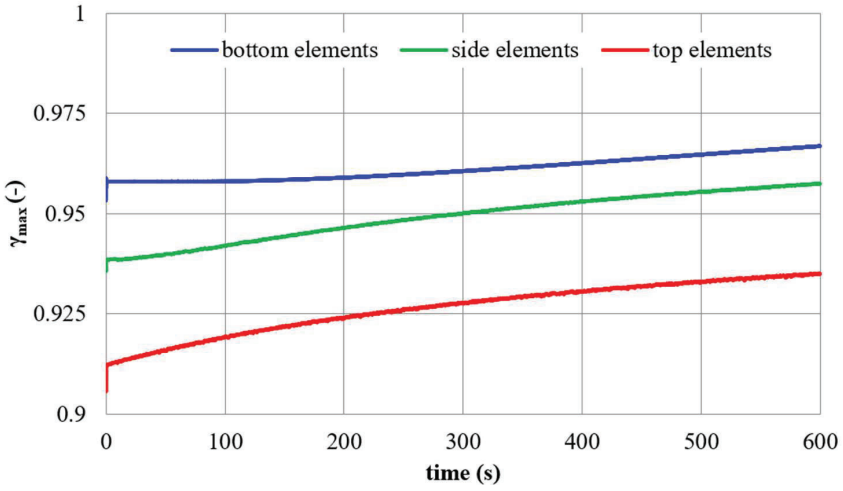

Figure 8: Temperature of the heating elements relative to their allowed maximum temperature.

5 CONCLUSIONS

To evaluate the behavior of an electrically heated tunnel kiln numerical simulations were performed. The goal was to prove whether the heating elements could withstand the temperatures in the most critical zone. Moreover, the product quality was assessed by evaluating the temperature distribution in the brick stack. The computational domain with around 22.5 million cells is proven to be numerical independent by GCI factors beneath 1%. A steady state simulation of the critical zone shows that the bottom elements reach temperatures around 4% below their lower fatigue limit. This is still within the desired range and can be considered as endurable. The transient simulation of around ten minutes within the critical zone also shows that all elements remain under the fatigue critical temperatures. Furthermore, the product quality with a maximum temperature spread in the brick stack of around 80K can be considered as comparable with natural gas-fired kilns.
To further improve the temperature gradient in the stack, going towards variability of the heating load managed by a control algorithm could be an option. Moreover, validation against experimental data is planned as the prototype will begin operation at the end of 2024.

NOMENCLATURE

Abbreviations

CFD	computational fluid dynamics
CFL	Courant-Friedrichs-Lewy number
GCI	grid convergence method/index
RANS	Reynolds averaged Navier Stokes equations
RE	Richardson extrapolation
URANS	unsteady Reynolds averaged Navier Stokes equations
S2S	surface-to-surface radiation model

Greek symbols

γ	temperature ratio between the heating element temperature in relation to its highest permissible operating temperature
φ	key variable for GCI method

Latin symbols

e	relative error
GCI	grid convergence index

https://doi.org/10.52202/077185-0135

h	representative cell size
N	number of cells
r	grid refinement factor

Subscripts

a	approximate
av	average
brick	brick
HE	heating element(s)
max	maximum
min	minimum

Superscripts

1, 2, 3	indexing for the fine, middle, and coarse grid in the grid independence study

REFERENCES

Abou-Ziyan, H., Almesri, I. F., Alrahmani, M. A., & Almutairi, J. H. (2018). Convective Heat Transfer Coefficients of Multifaceted Longitudinal and Transversal Bricks of Lattice Setting in Tunnel Kilns. *Journal of Thermal Science and Engineering Applications*, *10*(5). https://doi.org/10.1115/1.4040034.

ANSYS, Inc. (2022a). Ansys® Fluent Theory Guide, Release 2022 R1. Canonsburg, USA, 2022.

Celik, I., Ghia, U., Roache, P., Freitas, C., Coloman, H., and Raad, P. (2008). Procedure of estimation and reporting of uncertainty due to discretization in cfd applications. *Journal of Fluids Engineering*, 130:078001. https://doi.org/10.1115/1.2960953.

Krishna, S. (2021). Breaking the mold: a journey of the brick. Masters Thesis. *650*. https://digitalcommons.risd.edu/masterstheses/650.

Lee, M., Park, G., Park, C., and Kim, C. (2020). Improvement of grid independence test for computational fluid dynamics model of building based on grid resolution. *Advances in Civil Engineering,* 2020, 1-11. https://doi.org/10.1155/2020/8827936.

Menter, F. R. (1994). Two-equation eddy-viscosity turbulence models for engineering applications. *AIAA Journal*, 32(8):1598–1605. http://dx.doi.org/10.2514/3.12149.

Mödinger, F. (2021). Is hydrogen a viable fuel alternative for a traditional tunnel brick kiln? *Interceram - International Ceramic Review, 70(*1), 32–37.

Pichler, M., Wesenauer, F., Jordan, C., Puskas, S., Streibl, B., Winter, F., & Harasek, M. (2021). Design and simulation of gas burner ejectors. *Carbon Resources Conversion*, *4*, 28-35.

Puskas S., Jordan C., Pichler M., Wesenauer F., Streibl B., Winter F., & Harasek M. (2020). *Umwälzdüse für einen Brennofen* (Austria, Application no.: A50861/2020). Österreichisches Patentamt.

Refaey, H. A., & Specht, E. (2013). Flow field visualization to simulate the burning of sanitaryware in tunnel kilns. *Eleventh international conference of fluid dynamics, Alexandria, Egypt,* ICFD11.

Valdés, H., Vilches, J., Felmer, G., Hurtado, M. D. & Figueroa, J. D. (2020). Artisan Brick Kilns: State-of-the-Art and future Trends. *Sustainability, 12*(18), 7724. https://doi.org/10.3390/su12187724.

 https://doi.org/10.52202/077185-0135

ACKNOWLEDGEMENT

This publication has been conducted within the project „GreenBricks“ (FFG no. 999894581).
The project is supported with funds from the Climate and Energy Fund and implemented in the framework of the RTI-initiative “Flagship region Energy”.

https://doi.org/10.52202/077185-0135